Elucidation of Quasi-Duality between Series-Series and Series-Parallel Topologies of Resonant Inductive Coupling Wireless Power Transfer Systems

Masataka Ishihara, Kazuhiro Umetani, Eiji Hiraki
Graduate School of Natural Science and Technology
Okayama University
Okayama, Japan

Published in: 2017 IEEE 12th International Conference on
Power Electronics and Drive Systems (PEDS)

DOI: 10.1109/PEDS.2017.8289248

IEEE PEDS 2017, Honolulu, USA
12 – 15 December 2017

Elucidation of Quasi-Duality between Series-Series and Series-Parallel Topologies of Resonant Inductive Coupling Wireless Power Transfer Systems

Masataka Ishihara, Kazuhiro Umetani, Eiji Hiraki
Graduate School of Natural Science and Technology, Okayama University, Japan
p4wv0vf6@s.okayama-u.ac.jp

***Abstract*- Series-Series (SS) and Series-Parallel (SP) topologies are widely utilized in practical resonant inductive coupling wireless power transfer (RIC-WPT) systems owing to their simple circuit configurations. Conventionally, design optimization of the circuit parameters of these topologies were investigated separately, because these topologies are expressed by different equivalent circuits. However, analysis of these equivalent circuits is generally complicated due to the multiple resonant modes contained in the operation, which may cause difficulty in comparing the performance between the SS and SP topologies after design optimization of these topologies. This difficulty may prevent elucidating the methodology to select an appropriate topology that offers better output power or efficiency after design optimization. The purpose of this paper is to suggest a selection methodology of the SS and SP topologies by elucidating a novel insight that these topologies have the quasi-duality relation, in which the SP topology works approximately as the dual of the SS topology. This insight enables to share the analysis results between the topologies. As a result, both of these topologies were found to be expressed by a same novel equivalent circuit. Furthermore, the only difference between the SS and SP topologies were found to be the equivalent load resistance of this equivalent circuit, thus reducing the topology selection into selection of preferable load resistance. The appropriateness of the quasi-duality relation and the resultant equivalent circuit was successfully confirmed by the simulation and the experiment.**

I. INTRODUCTION

The resonant inductive coupling wireless power transfer (RIC-WPT) [1]–[11] has been attracting public attention as a high efficiency wireless power transfer technique for various applications such as electric vehicles [1]–[4], mobile devices, implanted biomedical devices [5], etc. Many wireless power transfer techniques utilize the magnetic induction between the magnetically coupled transmitting and receiving coils. However, the reactive impedance caused by the leakage inductance of these coils tends to restrict the current flow, preventing effective power transfer to the receiving coil. In the RIC-WPT system, this problem is addressed by adding a capacitor to each of the transmitting and receiving coils to cancel the reactive impedance [1]–[11]. Hence, the RIC-WPT is composed as the magnetically coupled transmitting and receiving resonators, as shown in Fig. 1, where W1 and W2 are the transmitting and receiving coils.

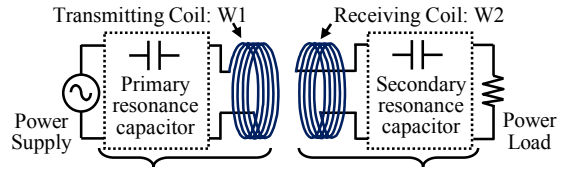

Fig. 1. Physical structure of RIC-WPT system.

In spite of this attractive feature, analysis of this technique is generally complicated because the operation contains multiple resonance modes. The RIC-WPT systems can be mainly classified into two topologies known as Series-Series (SS) and Series-Parallel (SP) topologies [1]–[5], [7]–[11], depending on the connection of the capacitor for the receiving side. However, these topologies have been analyzed and designed based on different equivalent circuits. Therefore, the complicated operating principle with multiple resonant modes prevents straightforward comparison of the circuit behavior between these topologies after design optimization of the circuit parameters, such as the leakage inductance of the coils, the capacitance of the resonant capacitors, and the load resistance. Consequently, selecting an appropriate topology according to the required specifications is generally difficult.

A key to solving this issue may lie in the duality [12]–[15] between these two topologies. The duality is often utilized in power electronics research for derivation of novel circuits [13] and analysis for the circuit behavior [14] [15]. The circuits under the duality relation is known to show the same circuit behavior except that the current and the voltage of the circuit elements are interchanged. This indicates that the performance of these circuits can be represented by the same equivalent circuit. Therefore, if there is a duality relation between the SS and SP topologies, the same analysis result of a single equivalent circuit can be shared between these two topologies. This may result in straightforward comparison of the output power and the efficiency after design optimization, probably leading to a selection method of the appropriate topology.

978-1-5090-2364-6/17/$31.00 ©2017 IEEE

As for the electric coupling wireless power transfer system, the SP and SS topologies have the quasi-duality relation and share the same equivalent circuit [14]. According to this equivalent circuit, the SP topology works as the dual of the SS topology in which the load resistance R is replaced by Z^2/R, where Z is the characteristic impedance of the transmitting and receiving resonators. (In [14], the same Z is assumed for these resonators.) This knowledge is promising because selecting a topology reduces in finding out which one of R and Z^2/R is preferable in the equivalent circuit.

Therefore, it is natural to suppose that the similar relation may also exist in the RIC-WPT. In fact, a previous study [10] suggested the possibility of the duality relation between the SS and the SP topologies of the RIC-WPT systems. This previous study pointed out that the frequency characteristics of the voltage gain and the current gain seem to be interchanged between the SS and SP topologies. However, discussion of the previous study has been limited to pointing out the analogy between these two topologies. If this duality relation is theoretically proven, the performance of the SS and SP topologies can be analyzed according to the same equivalent circuit and the analysis result may be easily compared each other. Hence the duality between these two topologies may offer a simple strategy for selecting an appropriate topology.

The purpose of this paper is to elucidate the duality relation of the RIC-WPT systems. Similarly, as in [14], the duality is investigated by comparing the equivalent circuits of the SS and SP topologies derived using the Lagrangian dynamics. Lagrangian dynamics [16] [17] was employed because this dynamics has recently been proven to be effective for deriving various equivalent circuits that cannot be derived using the conventional circuit theory. Then, based on this duality relation, this paper further derives a novel equivalent circuit can represent both of the SS and SP topologies. As a result, this paper elucidates that the efficiency and the output power of the SP topology can be approximated as those of the SS topology in which only the load resistance was changed.

The following discussion consists of five sections. Section II and Section III derive the Lagrangian equivalent circuit for the SS and SP topologies, respectively. Based on these Lagrangian equivalent circuits, section IV derives and analyses the novel equivalent circuit that represents both of the SS and SP topologies. Section V presents simulation and experiment to verify the analysis results of the equivalent circuit. Finally, section VI presents the conclusions.

II. Equivalent Circuit of SS Topology

This section derives the equivalent circuit of the SS topology shown in Fig. 2 using Lagrangian dynamics. Symbol E is the voltage of the power supply; R is the resistance of the power load; N_1 and N_2 are the number of turns of W1 and W2, respectively; r_1 and r_2 are the parasitic resistance of W1 and W2, respectively; P_1, P_2, and P_M are the permeance of the magnetic path for the flux ϕ_1, ϕ_2, and ϕ_M, respectively; C_1 and C_2 are the capacitance.

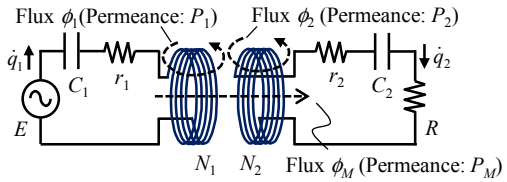

Fig. 2. Circuit model of SS topology.

The leakage inductance of W1 and W2 (L_{leak1} and L_{leak2}), the mutual inductance between W1 and W2 (M), the self-inductance of W1 and W2 (L_1 and L_2), and coupling coefficient k are defined as

$$\begin{aligned} &L_{leak1} = N_1{}^2 P_1, \quad L_{leak2} = N_2{}^2 P_2, \quad M = N_1 N_2 P_M, \\ &L_1 = L_{leak1} + \frac{N_1}{N_2} M, \quad L_2 = L_{leak2} + \frac{N_2}{N_1} M, \quad k = \frac{M}{\sqrt{L_1 L_2}}. \end{aligned} \tag{1}$$

We assume that the resonance frequency is the same in the transmitting and receiving resonators as is natural for common design of the RIC-WPT systems. Assuming weak magnetic coupling between the transmitting and receiving coils, we impose $L_{leak1}C_1 \approx L_{leak2}C_2$ because the self-inductance of W1 and W2 are approximately equal to the leakage inductance of W1 and W2 under small coupling coefficient k.

The Lagrangian derivation process of the equivalent circuit can be divided into the following three steps. First, the Lagrangian model of the circuit model is configured. The Lagrangian model consists of the Lagrangian and the dissipation function. Second, the Lagrangian model is applied with a coordinate transformation to obtain another Lagrangian model belonging to a different circuit topology. The coordinate transformation is known to conserve the circuit behavior represented by the Lagrangian model. Hence, this step yields a Lagrangian model of an equivalent circuit. Third, the resultant Lagrangian model is translated into a circuit diagram, yielding a Lagrangian equivalent circuit.

Now, we construct the Lagrangian model based on the circuit model of the SS topology. According to the method described in [16], Fig. 2 can be translated into the Lagrangian Λ_{SS} and the dissipation function D_{SS} as

$$\begin{aligned} \Lambda_{SS} = {} & N_1 \dot{q}_1 (\phi_1 + \phi_M) + N_2 \dot{q}_2 (\phi_2 - \phi_M) - \phi_1{}^2 / 2P_1 \\ & - \phi_2{}^2 / 2P_2 - \phi_M{}^2 / 2P_M - q_1{}^2 / 2C_1 - q_2{}^2 / 2C_2 + E q_1, \end{aligned} \tag{2}$$

$$D_{SS} = R \dot{q}_2{}^2 / 2 + r_1 \dot{q}_1{}^2 / 2 + r_2 \dot{q}_2{}^2 / 2, \tag{3}$$

where q_1 and q_2 are the time integration of the current; and a dot over a variable indicates its time derivative.

Next, a coordinate transformation is applied to (2) and (3), as exemplified in [14] [17]. For this purpose, we introduce new variables q_A, q_B, ϕ_A, and ϕ_B defined as

$$\begin{aligned} &q_A = \frac{\alpha (N_2 C_2 q_1 + N_1 C_1 q_2)}{2 N_1 C_1}, \quad q_B = \frac{\beta (N_1 q_1 - N_2 q_2)}{2 N_2}, \\ &\phi_A = P_1 (\phi_1 + \phi_2) / (P_1 + P_2), \quad \phi_B = (P_2 \phi_1 - P_1 \phi_2) / (P_1 + P_2), \end{aligned} \tag{4}$$

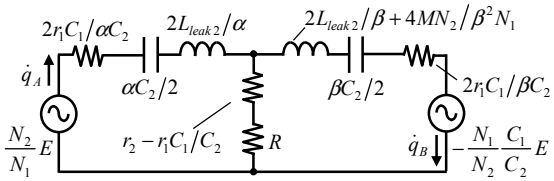

Fig. 3. Lagrangian equivalent circuit of SS topology.

where the dimensionless quantity α and β are defined as

$$\alpha=\frac{2N_1^2C_1}{N_1^2C_1+N_2^2C_2},\quad \beta=\frac{2N_2^2C_2}{N_1^2C_1+N_2^2C_2}. \tag{5}$$

Substituting (4) into (2) and (3) yields

$$\begin{aligned}\Lambda_{SS}&=2N_2\left(\dot{q}_A\phi_A+\dot{q}_B\phi_B+\dot{q}_B\phi_M\right)/\beta-q_A^2/\alpha C_1\\&\quad-q_B^2/\beta C_2-\phi_A^2/\beta P_1-\phi_B^2/\beta P_2-\phi_M^2/2P_M\\&\quad+Eq_AN_2/N_1+Eq_BN_1C_1/N_2C_2.\end{aligned} \tag{6}$$

$$\begin{aligned}D_{SS}&=R\left(\dot{q}_A-\dot{q}_B\right)^2/2+C_1r_1/C_2\left(\dot{q}_A/\alpha+\dot{q}_B/\beta\right)\\&\quad+\left(C_2r_2-C_1r_1\right)\left(\dot{q}_A-\dot{q}_B\right)^2/2C_2.\end{aligned} \tag{7}$$

For derivation of (6) and (7), we utilized the approximation that $L_{leak1}C_1\approx L_{leak2}C_2$. By translating (6) and (7) into a circuit model, the equivalent circuit for the SS topology is obtained as shown in Fig. 3.

Note that the output power as well as the total input power supplied from the AC voltage source is the same between Fig. 2 and Fig. 3 because the coordinate transformation in the Lagrangian model conserves the energy [16]. Hence, the efficiency is also conserved in the equivalent circuit.

III. Equivalent Circuit of SP Topology

Next, this section derives the equivalent circuit of the SP topology shown Fig. 4. In the SP topology, the capacitor is connected in parallel to the receiving coil. Similarly, as in the previous section, the Lagrangian Λ_{SP} and the dissipation function D_{SP} of Fig. 4 can be constructed as

$$\begin{aligned}\Lambda_{SP}&=N_1\dot{q}_1\left(\phi_1+\phi_M\right)+N_2\left(\dot{q}_2+\dot{q}_R\right)\left(\phi_2-\phi_M\right)-\phi_1^2/2P_1\\&\quad-\phi_2^2/2P_2-\phi_M^2/2P_M-q_1^2/2C_1-q_2^2/2C_2+Eq_1,\end{aligned} \tag{8}$$

$$D_{SP}=R\dot{q}_R^2/2+r_1\dot{q}_1^2/2+r_2\left(\dot{q}_2+\dot{q}_R\right)^2/2. \tag{9}$$

Then, we introduce new variables q_a, q_b, q_c, ϕ_a, and ϕ_b defined as

$$\begin{aligned}&q_a=\frac{N_2C_2q_1+N_1C_1q_2}{2N_1C_1},\quad q_b=\frac{N_1q_1-N_2q_2}{2N_2},\\&q_c=\frac{q_R}{2},\quad \phi_a=\frac{2P_2\left(\phi_1+\phi_2\right)}{P_1+P_2},\quad \phi_b=\frac{2\left(P_2\phi_1-P_1\phi_2\right)}{P_1+P_2}.\end{aligned} \tag{10}$$

Substituting (10) into (8) and (9) yields

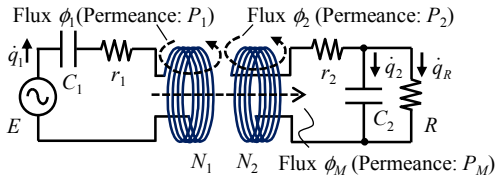

Fig. 4. Circuit model of SP topology.

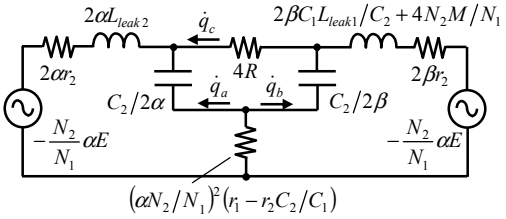

Fig. 5. Lagrangian equivalent circuit of SP topology.

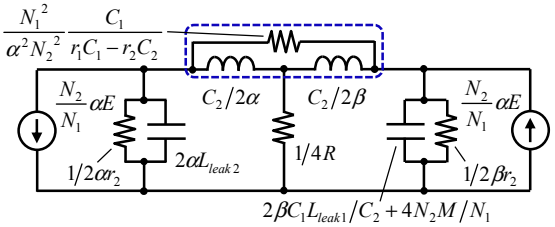

Fig. 6. Dual circuit of Fig. 5.

$$\begin{aligned}\Lambda_{SP}&=N_2\left\{\left(\dot{q}_a+\dot{q}_c\right)\phi_a+\left(\dot{q}_b-\dot{q}_c\right)\phi_b+2\left(\dot{q}_b-\dot{q}_c\right)\phi_M\right\}\\&\quad-\alpha q_a^2/C_2-\beta q_b^2/C_2-\phi_a^2/4\alpha P_2-\phi_b^2/4\alpha P_1\\&\quad-\phi_M^2/2P_M+\alpha N_2E\left(q_a+q_b\right)/N_1,\end{aligned} \tag{11}$$

$$\begin{aligned}D_{SP}&=2R\dot{q}_c^2+\alpha r_2\left(\dot{q}_a+\dot{q}_c\right)^2+\beta r_2\left(\dot{q}_b-\dot{q}_c\right)^2\\&\quad+\left(\alpha N_1/N_2\right)^2\left(C_1r_1-C_2r_2\right)\left(\dot{q}_a+\dot{q}_b\right)^2/2C_1.\end{aligned} \tag{12}$$

Similarly, as in the previous section, by translating (11) and (12), we can obtain the equivalent circuit, shown in Fig. 5. The power as well as the efficiency is conserved in the equivalent circuit, similarly as in section II.

IV. Analysis of Equivalent Circuits

As shown above, Fig. 5 has far different network from Fig. 3. However, these two Lagrangian equivalent circuits have the quasi-duality relation. This subsection elucidates this relation by analyzing the Lagrangian equivalent circuits.

First, we apply the duality transformation to the Lagrangian equivalent circuit of the SP topology, i.e. Fig. 5. As a result, we obtain the dual of Fig. 5, as shown in Fig. 6.

Second, we further apply the Δ-Y transformation to the sub-circuit marked by the dashed line in Fig. 6. Furthermore, after applying the Δ-Y transformation, we introduce the following practically acceptable two approximations in addition to the already introduced approximation of $L_{leak1}C_1\approx L_{leak2}C_2$.

1. The frequency region to be discussed is assumed to be in the vicinity of the resonance frequency of the transmitting and receiving resonators. Hence, $\omega^2\approx 1/L_1C_1\approx 1/L_2C_2$.

2. The quality factor of the transmitting and receiving resonators are far greater than 1. Hence, $\omega L_{leak1}/r_1>>1$ and $\omega L_{leak2}/r_2>>1$.

By applying the Δ-Y transformation as well as the aforementioned approximation, we obtain Fig. 7.

Third, we further apply Thevenin's theorem to the sub-circuit marked by the dashed line in Fig. 7, to obtain Fig. 8. This transformation conserves the output power. However, the input power is not strictly conserved because the input power in Fig. 8 does not entirely contains the power consumed at the resistance $1/2\alpha r_2$ in Fig. 7. However, according to the assumption of large quality factor, we can approximate that the current across the resistor $1/2\alpha r_2$ is sufficiently small and the input energy in Fig. 8 is almost the same as that in Fig. 7. Consequently, the input and the output energy can be approximated to be the same between Fig. 7 and Fig. 8.

Fourth, we apply an impedance transformation to Fig 8. Specifically, we multiply the voltage and current in the circuit, by $2Z$ and $1/2Z$, respectively, where Z is the characteristic impedance of the receiving resonator defined as $Z^2 \equiv L_2/C_2 \approx L_{leak2}/C_2$. ($L_2$ is the self-inductance of W2.) As a result, Fig. 8 is transformed into Fig. 9. Because this transformation also conserves the energy, the input and output power is the same between Fig. 8 and Fig. 9.

Fifth, by applying the approximation introduced above, we transform the sub-circuit marked by the dashed lines in Fig. 9. The amplitude of the voltage sources marked by the red (i) and blue (ii) dashed lines can be respectively approximated as

$$\begin{aligned} &-\frac{N_2}{N_1}\frac{ZE}{j\omega L_{leak2}+r_2} = -\frac{N_2}{N_1}\sqrt{\frac{L_2}{C_2}}\frac{E}{j\omega L_{leak2}+r_2} \\ &\approx -\frac{N_2}{N_1}\sqrt{\frac{L_{leak2}}{C_2}}\frac{E}{j\omega L_{leak2}} \approx j\frac{N_2}{N_1}E, \end{aligned} \tag{13}$$

$$\begin{aligned} &\frac{\alpha ZE}{j\omega\left(\alpha L_{leak1}N_2/N_1+2M\right)} \approx \frac{N_1}{N_2}\sqrt{\frac{L_2}{C_2}}\frac{E}{j\omega L_{leak1}} \\ &\approx \frac{N_1}{N_2}\sqrt{\frac{L_2}{C_2}}\sqrt{\frac{C_1}{L_1}}(-jE) \approx -j\frac{N_1}{N_2}\frac{C_1}{C_2}E. \end{aligned} \tag{14}$$

In addition, the impedance marked by the green (iii) dashed lines Z_l can be represented as

$$Z_l = 1\Big/\left(\frac{\alpha r_2}{2Z^2}+j\omega\frac{\alpha L_{leak2}}{2Z^2}\right)+\frac{2}{\alpha}\left(\frac{C_1}{C_2}r_1-r_2\right)+j\omega\frac{2L_2}{\alpha}. \tag{15}$$

The first term in the right-hand side of (15) can be approximated as

$$\begin{aligned} &1\Big/\left(\frac{\alpha r_2}{2Z^2}+j\omega\frac{\alpha L_{leak2}}{2Z^2}\right) \approx \frac{2Z^2}{\alpha}\frac{r_2-j\omega L_2}{{r_2}^2+\omega^2{L_2}^2} \\ &\approx \frac{2Z^2}{\alpha}\frac{r_2}{\omega^2{L_2}^2}+\frac{2Z^2}{\alpha}\frac{1}{j\omega L_2} \approx \frac{2}{\alpha}\left(r_2+\frac{1}{j\omega C_2}\right). \end{aligned} \tag{16}$$

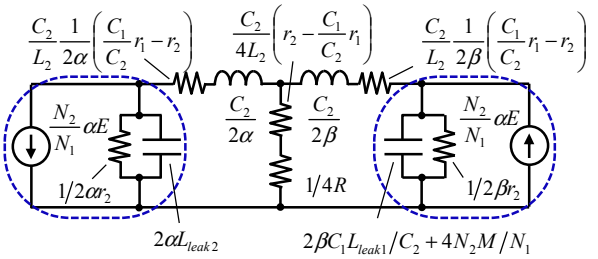

Fig. 7. Equivalent circuit applying Δ-Y transformation to Fig. 6.

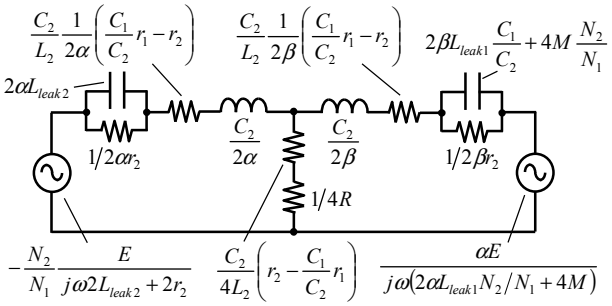

Fig. 8. Equivalent circuit applying Thevenin's theorem to Fig. 7.

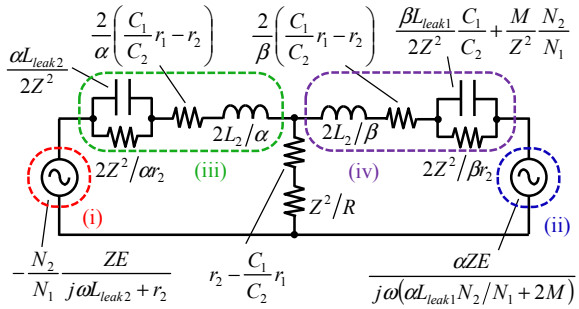

Fig. 9. Result of the impedance transformation of Fig. 8.

Substituting (16) into (15) yields

$$Z_l \approx (2/\alpha)\left(r_1C_1/C_2+1/j\omega C_2+j\omega L_{leak2}\right). \tag{17}$$

Similarly, the impedance marked by the purple (iv) dashed lines Z_r can be represented as

$$\begin{aligned} Z_r &= j\omega\frac{2L_2}{\beta}+\frac{2}{\beta}\left(\frac{C_1}{C_2}r_1-r_2\right) \\ &+1\Big/\left\{\frac{\beta r_2}{2Z^2}+j\omega\left(\frac{\beta L_{leak1}}{2Z^2}\frac{C_1}{C_2}+\frac{M}{Z^2}\frac{N_2}{N_1}\right)\right\}. \end{aligned} \tag{18}$$

The first and third terms in the right-hand side of (18) can be respectively approximated as

$$\begin{aligned} &j2\omega L_2/\beta = j2\omega L_{leak2}/\beta+j2\omega(N_2/N_1)M/\beta \\ &\approx j2\omega L_{leak2}/\beta+j4\omega(N_2/N_1)M/\beta^2, \end{aligned} \tag{19}$$

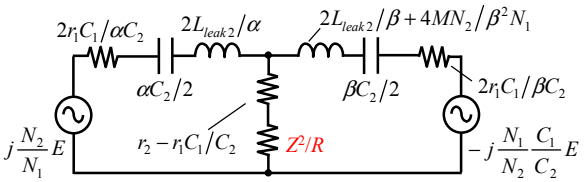

Fig. 10. Approximated equivalent dual circuit based on Fig. 9.

$$1\Big/\left\{\frac{\beta r_2}{2Z^2}+j\omega\left(\frac{\beta L_{leak1}}{2Z^2}\frac{C_1}{C_2}+\frac{M}{Z^2}\frac{N_2}{N_1}\right)\right\}$$
$$\approx 1\Big/\frac{\beta}{2Z^2}\left\{r_2+j\omega\left(L_2+\frac{2}{\beta}\frac{N_2}{N_1}M\right)\right\}\approx\frac{2Z^2}{\beta}\frac{1}{r_2+j\omega L_2} \quad (20)$$
$$\approx\left(2Z^2/\beta\right)\left(r_2/\omega^2{L_2}^2-j/\omega L_2\right)\approx\left(2/\beta\right)\left(r_2+1/j\omega C_2\right).$$

Substituting (19) and (20) into (18) yields

$$Z_r=j\omega\left(\frac{2L_{leak2}}{\beta}+\frac{4}{\beta^2}\frac{N_2}{N_1}M\right)+\frac{2}{\beta}\frac{C_1}{C_2}r_1+\frac{2}{\beta}\frac{1}{j\omega C_2}. \quad (21)$$

Approximating the AC voltage by (13) and (14) and expressing the impedance (17) and (21) as series-connected resistor, capacitor, and inductor, we can approximate Fig. 9 as Fig. 10. Throughout the derivation process of Fig. 10, the input and the output power (and therefore, the efficiency) is almost conserved. Hence, Fig. 10 works approximately an equivalent dual circuit of the SP topology.

As can be seen in Fig. 3 and Fig. 10, these circuits have the same topology. Furthermore, the circuit parameters are also the same except for the load resistance. Therefore, the SP topology approximately works as the dual of the SS topology in which the load resistance R is replaced by Z^2/R, similarly as in the electric coupling wireless power transfer system. We term this relation as the quasi-duality because some approximations were used to prove the duality.

This insight may be effective for selecting an appropriate topology from the SS and SP topologies. According to this quasi-duality, the only difference between the SS and SP topologies is the load resistance from the viewpoint of the efficiency and the output power. Hence, we can select the topology by finding out which one of R and Z^2/R is preferable, i.e. leads to higher efficiency or larger output power, for the load resistance of the SS topology. (Note that Fig. 3 is the equivalent circuit of the SS topology.)

As widely known, the SS topology has an appropriate load resistance value that maximizes the efficiency or the output power. Hence, preferable load resistance may be chosen which one of R and Z^2/R is closer to this appropriate load resistance.

V. Simulation and Experimental Results

This section evaluates the quasi-duality by the simulation and the experiment. As for the simulation, we calculated the behavior of the circuit models shown in Fig. 2 and Fig. 4 using the circuit simulator LTspice XII. Circuit parameters for these models are the same except for the load resistance. We set the load resistance R_{SP} for Fig. 4, i.e. the SP topology, at Z^2/R_{SS}, where R_{SS} is the load resistance of Fig. 2, the SS topology. Then, we compared the simulated frequency dependence of the input and output power between Fig. 2 and Fig. 4.

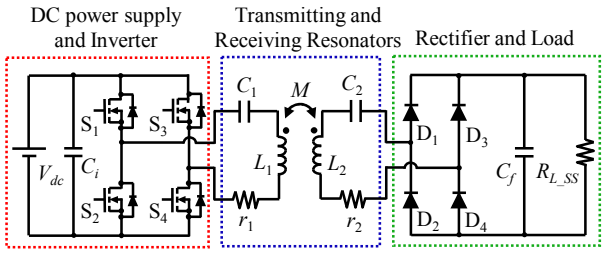

Fig. 11. Circuit diagram of SS topology.

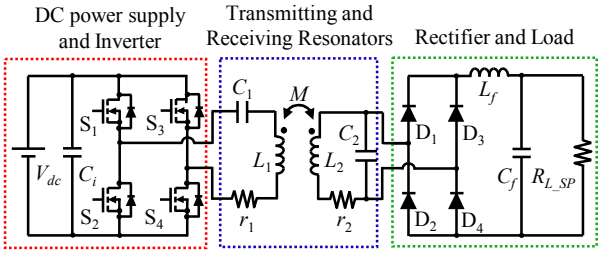

Fig. 12. Circuit diagram of SP topology.

TABLE I
Circuit Parameters of SS and SP Topologies

Input DC voltage	V_{dc}	35 V
Self-inductance of primary side	L_1	141.27 µH
Parasitic resistance of primary side	r_1	0.156 Ω
Capacitance of primary side	C_1	16.14 nF
Self-inductance of secondary side	L_2	55.60 µH
Parasitic resistance of secondary side	r_2	0.080 Ω
Capacitance of secondary side	C_2	40.80 nF
Mutual inductance	M	5.3 µH

On the other hand, we experimentally evaluated the input and output power using the prototypes of the SS and SP topologies. The circuit diagram of these prototypes are shown in Fig. 11 and Fig. 12. These prototypes are also designed to have the same circuit parameters except for the load resistance, which was set to have the relation of $R_{SP}=Z^2/R_{SS}$. Then, we also compared the measured frequency dependence of the input and output power between these topologies.

The circuit parameters of the experimental prototypes are shown in Table I. The same parameters are utilized for the simulation. Certainly, the prototypes have the square-wave voltage source generated by the full-bridge inverter, whereas the simulation assumes the sinusoidal AC voltage source. However, the amplitude of the AC voltage source in the simulation models was set at the amplitude of the fundamental wave [8] extracted from the square-wave voltage source of the prototypes. Furthermore, the load resistance of the simulation was set at the equivalent AC resistance [18] of the load R_{L_SS} and R_{L_SP} including the rectifier.

Fig. 13 and Fig. 14 show the simulation and experimental results of the input and output power, respectively. The solid lines indicate the simulation results, whereas the makers indicate the experimental results. As can be seen from Fig. 13 and Fig. 14, both the simulation and the experiment revealed

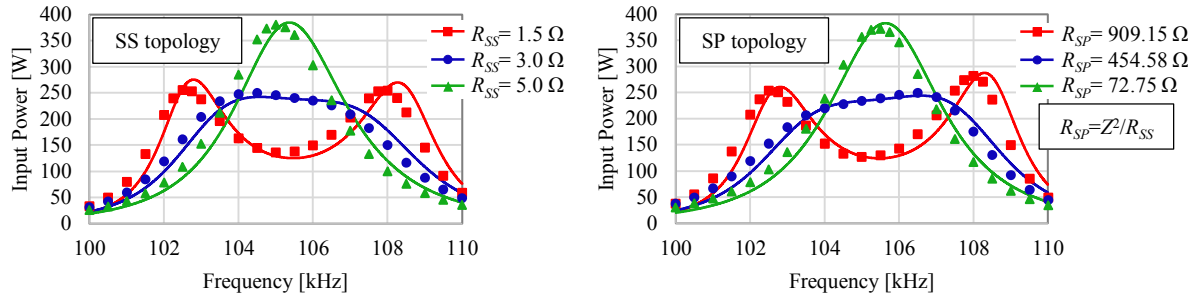

Fig. 13. Simulation and experimental results of input power.

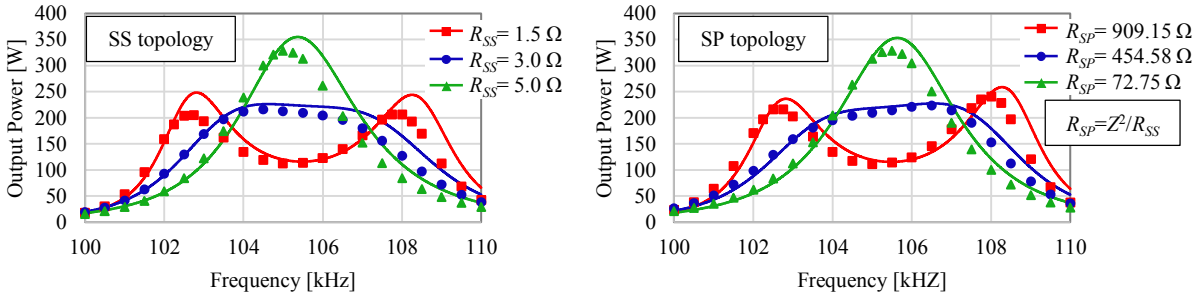

Fig. 14. Simulation and experimental results of output power.

that the SS and SP topologies have almost the same frequency dependence of the input and output power. This indicates appropriateness of the quasi-duality between the SS and SP topologies under the condition of R_{SP}=Z^2/R_{SS}.

VI. Conclusion

This paper investigated the quasi-duality between the SS and SP topologies of the RIC-WPT system. As a result, the SP topology was found to operate approximately as the dual of the SS topology with the transformed load resistance. This quasi-duality was verified by the simulation and the experiment. This insight implies that an appropriate topology can be selected for practical applications by finding out which of the original load resistance or the transformed load resistance is preferable for the SS topology.

Acknowledgment

This work was supported by The Institute of Electrical Engineers of Japan Chugoku Branch.

References

[1] C.-S. Wang, G. A. Covic, and O. H. Stielau, "Power transfer capability and bifurcation phenomena of loosely coupled inductive power transfer systems," *IEEE Trans. Ind. Electron.*, vol. 51, issue. 1, pp. 148–157, Feb. 2004.

[2] S. Li, and C. C. Mi, "Wireless power transfer for electric vehicle applications," *IEEE Trans. Emerg. Sel. Topics Power Electron.*, vol. 3, issue. 1, pp. 4–17, Mar. 2015.

[3] N. Liu, and T. G. Habetler, "Design of a universal inductive charger for multiple electric vehicle models," *IEEE Trans. Power Electron.*, vol. 30, issue. 11, pp. 6378–6390, Nov. 2015.

[4] C.-S. Wang, O. H. Stielau, and G. A. Covic, "Design considerations for a contactless electric vehicle battery charger," *IEEE Trans. Ind. Electron.*, vol. 52, issue. 5, pp. 1308–1314, Oct. 2005.

[5] I. O.-Isasa, K. P. Benli, F. Casado, J. I. Sancho, and D. Valderas, "Topology analysis of wireless power transfer systems manufactured via inkjet printing technology," *IEEE Trans. Ind. Electron.*, to be published.

[6] W.-Q. Niu, J.-X. Chu, W. Gu, and A.-D. Shen, "Exact analysis of frequency splitting phenomena of contactless power transfer systems," *IEEE Trans. Circuits Syst. I, Reg. Papers.*, vol. 60, issue. 6, pp. 1670–1677, June. 2013.

[7] M. Kim, J.-W. Lee, and B. K. Lee, "Practical bifurcation criteria considering inductive power pad losses in wireless power transfer Systems," *J. Electr Eng Technol.*, vol. 12, no. 1, pp. 173–181, Jan. 2017.

[8] H. Matsumoto, Y. Neba, and H. Asahara, "Switched compensator for contactless power transfer systems," *IEEE Trans. Power Electron.*, vol. 30, issue. 11, pp. 6120–6129, Nov. 2015.

[9] W. Zhang, S.-C. Wong, C. K. Tse, and Q. Chen, "Analysis and comparison of secondary series- and parallel-compensated inductive power transfer systems operating for optimal efficiency and load-independent voltage-transfer ratio," *IEEE Trans. Power Electron.*, vol. 29, no. 6, pp. 2979–2990, June. 2014.

[10] W. Zhang, S.-C. Wong, C. K. Tse, and Q. Chen, "Load-independent duality of current and voltage outputs of a series- or parallel-compensated inductive power transfer converter with optimized efficiency," *IEEE Trans. Emerg. Sel. Topics Power Electron.*, vol. 3, issue. 1, pp. 137–146, Mar. 2015.

[11] R. Jegadeesan, and Y.-X. Guo, "Topology selection and efficiency improvement of inductive power links," *IEEE Trans. Antennas Propag.*, vol. 60, issue. 10, pp. 4846–4854, Oct. 2012.

[12] S. D. Freeland, "Techniques for the practical application of duality to power circuits," *IEEE Trans. Power Electron.*, vol. 7, issue. 2, pp. 374–384, Apr. 1992.

[13] Z. H. Bai, and Z. C. Zhang, "Conformation of multilevel current source converter topologies using the duality principle," *IEEE Trans. Power Electron.*, vol. 23, issue. 5, pp. 2260–2267, Sept. 2008.

[14] M. Ishihara, K. Umetani, H. Umegami, E. Hiraki, and M. Yamamoto, "Quasi-duality between SS and SP topologies of basic electric-field coupling wireless power transfer system," *IET. Electron. Lett.*, vol. 52, issue. 25, pp. 2057–2059, Dec. 2016.

[15] J. W. Kolar, H. Ertl, and F. Zach, "Quasi-dual modulation of three-phase PWM converters," *IEEE Trans. Ind. Appl.*, vol. 29, issue. 2, pp. 313–319, Mar.–Apr. 1993.

[16] K. Umetani, "A generalized method for Lagrangian modeling of power conversion circuit with integrated magnetic components," *IEEJ Trans. Elect. Electron. Eng.*, vol. 7, issue. S1, pp. S146–S152, Dec. 2012.

[17] K. Umetani, J. Imaoka, M. Yamamoto, S. Arimura, and T. Hirano, "Evaluation of the Lagrangian method for deriving equivalent circuits of integrated magnetic components: a case study using the integrated winding coupled inductor," *IEEE Trans. Ind. Appl.*, vol. 51, no. 1, pp. 547–555, Jan.–Feb. 2015.

[18] R. L. Steigerwald, "A comparison of half-bridge resonant converter topologies," *IEEE Trans. Power Electron.*, vol. 3, issue. 2, pp. 174–182, Apr. 1988.